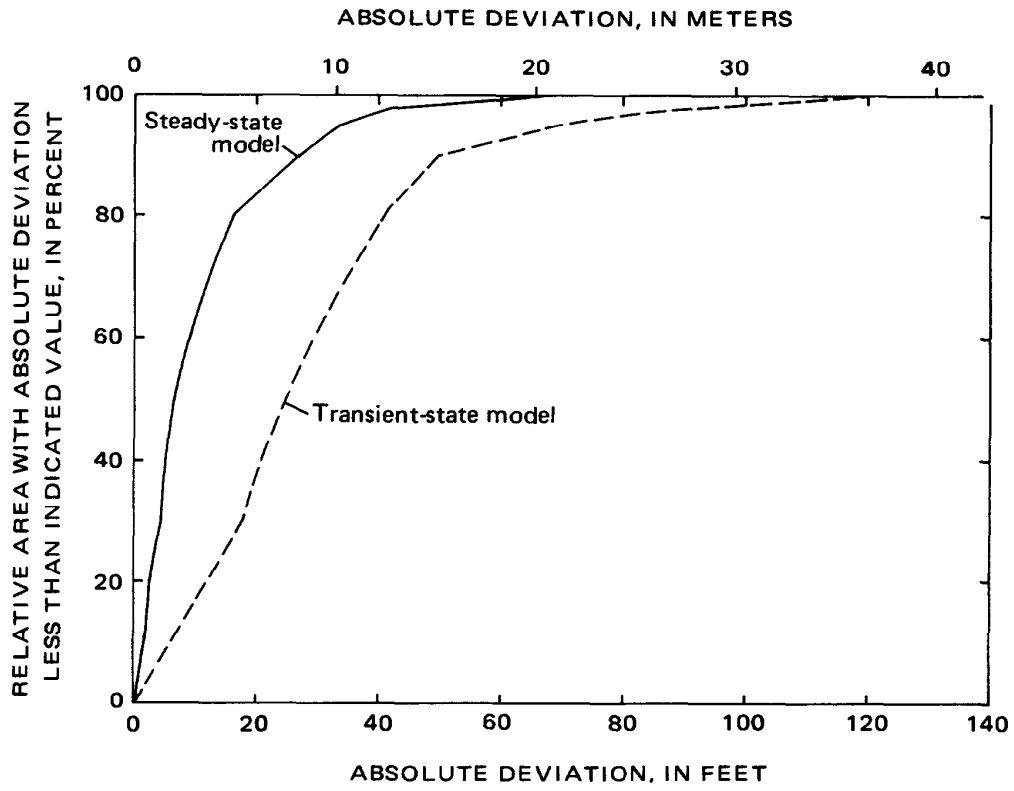

FIGURE 6.—Relative cumulative distribution of the absolute deviation of the computed hydraulic head from the prototype water level for the principal aquifer within the Lancaster subbasin.

basin is intended to represent temporal changes of water levels in the basin. The input to the model is natural recharge of ground water (which was presumed to be the same as the natural recharge that was used in the steady-state model), pumpage of ground water, irrigation return, and the reduction of natural discharge. The output from the model is the change of hydraulic head with time in the principal and deep aquifers. The calibration problem for this model was the modification of prior estimates of the storage coefficient of the aquifers.

PUMPAGE

In Antelope Valley the use of ground water for agricultural purposes began in about 1880, when it was discovered that wells drilled in the lower part of the valley yielded flowing water in quantities sufficient for irrigation (Thompson, 1929). In 1891 more than 100 wells were in use, but by that time only a few wells were flowing (R. J. Henton, as cited in Wright, 1924). Drilling of large numbers of wells began shortly before 1920 (Wright, 1924). Data presented by Snyder (1955) indicate a rapid increase in the number of wells immediately after that date; hence, it seems that the effective beginning of ground-water use in Antelope Valley is 1915.

As the number of wells in Antelope Valley increased, the quantity of water discharged by wells also increased. In 1924 about 55,000 acre-ft (68 hm^3) of water was pumped. By 1930 the annual pumpage had increased to 170,000 acre-ft (210 hm^3) (Snyder, 1955). During the period of economic depression following 1930, pumpage declined until in 1933 the annual pumpage was about 95,000 acre-ft (117 hm^3). After 1933, pumpage again increased until about 1950, when the annual pumpage reached the highest value of about 300,000 acre-ft (400 hm^3) (Snyder, 1955; California State Water Resources Control Board, 1974). Declining water levels resulted in uneconomically high pumping lifts in some parts of Antelope Valley, and pumpage again declined after 1950. In 1972 the annual pumpage was about 200,000 acre-ft (200 hm^3) (K. W. Mido, California Department of Water Resources, written commun., 1973).

Long-term changes in the pumping rate usually correspond to changes in the acreage under irrigation in Antelope Valley. An increase in pumpage usually means that new land has been brought under irrigation; a decrease in pumpage means that land has been removed from irrigation. At the time of the highest pumping rate, about 70,000 acres (28,000 ha) of land were under irrigation (Snyder, 1955). At that time the irrigated land in Antelope Valley was mostly in the Lancaster subbasin. About two-thirds of the irrigated land was in the eastern part of the subbasin, and the remaining irrigated land was in the western part. The central part of the Lancaster subbasin has not been extensively irrigated.

On the basis of data presented by California Department of Water Resources (1947; K. W. Mido, written commun., 1973), the geographic distribution of irrigated land and of pumpage (pl. 10) in Antelope Valley remained generally unchanged from 1915 through 1961, although local changes in both did occur. After about 1961 the geographic distribution of irrigated land changed. The centroid of irrigated land in the eastern part of the Lancaster subbasin moved about 10 mi (16 km) south of its former position, and the centroid of irrigated land in the western part of the subbasin moved about 10 mi (16 km) north of its former position. These shifts in the geographic distribution of irrigated land were related in part to the decline of ground-water levels in the Lancaster subbasin; irrigation was abandoned where pumping lifts became uneconomically high.

Snyder (1955), California Department of Water Resources (K. W. Mido, written commun., 1973), California State Water Resources Control Board (1974), and Antelope Valley-East Kern Water Agency (W. G. Spinarski, written commun., 1976) have estimated the annual pumpage in Antelope Valley for periods ranging from 1 to 28 years (fig. 7). The estimates of pumpage that were made by these different

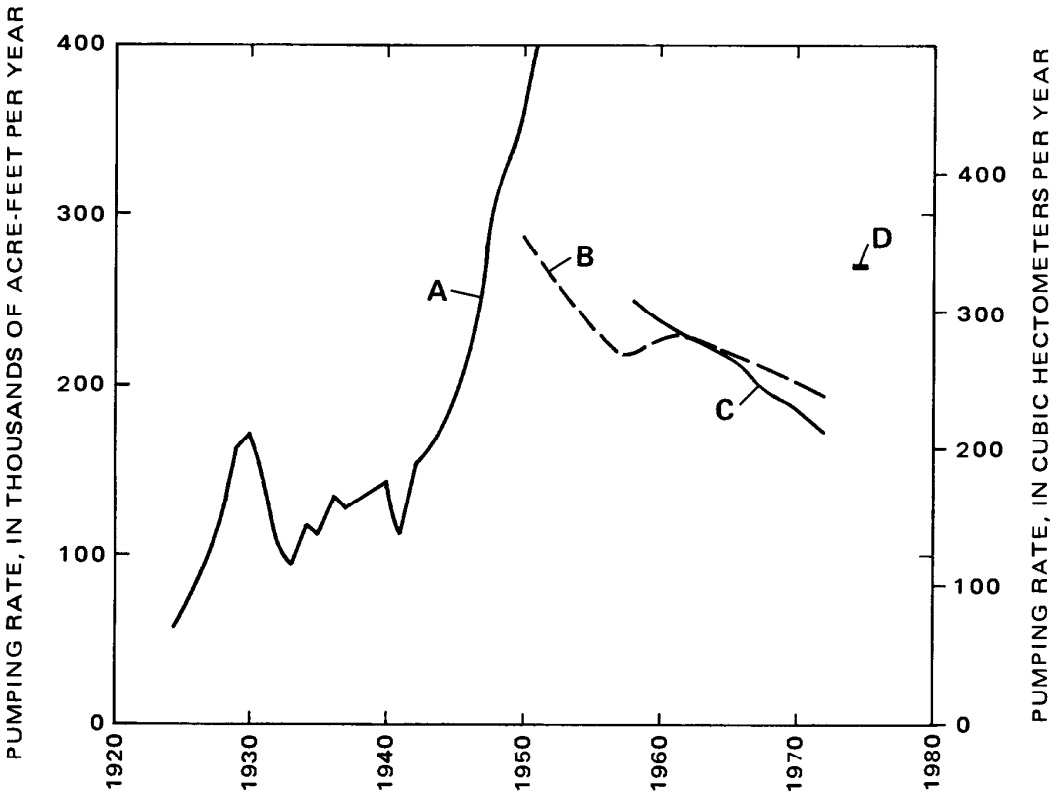

FIGURE 7.—Previous estimates of the temporal distribution of pumpage. Curve A is the estimate by Snyder (1955). Curve B is the estimate by California State Water Resources Control Board (1974). Curve C is the estimate by California Department of Water Resources (K. W. Mido, written commun., 1973). Curve D is the estimate by Antelope Valley-East Kern Water Agency (W. G. Spinarski, written commun., 1976).

investigators do not agree where the periods covered by the estimates are coincident. For example, Snyder (1955) estimated that the annual pumpage in 1950 was 362,000 acre-ft (446 hm^3), and California State Water Resources Control Board (1974) reported this pumpage to be 285,000 acre-ft (351 hm^3).

The data shown in figure 7 are only estimates of the true pumpage, and individual data points would be expected to deviate from the true pumpage. If, however, the pumpage used in the calibration of the transient-state model deviates from the true value, the estimates of the storage-coefficient values obtained from the calibration most likely will also deviate from the true values. Thus, it becomes important to devise a method that will allow estimation of the pumpage as accurately as possible.

A commonly used method for improving estimates of a quantity is to average several estimates. This average is, as are the original estimates on which it is based, only an approximation of the true value. The probable deviation of the average from the true value,

however, will generally be smaller than the probable deviation of any one of the original estimates from the true value.

The pumpage curve A in figure 8 represents an average of the pumpage data shown in figure 7. This curve was constructed by giving approximately equal weight to the curves A, B, C, and D in figure 7 (curve D was extrapolated backward in time parallel to general trend of curves B and C until it intersected curve A). Other estimates of the true pumpage can be obtained by giving unequal weight to the available data. Curve B in figure 8 represents an unequally weighted average of the data in figure 7. For this average, little weight was given to curve D because of the short time interval covered by the estimate.

By giving different weights to the available data, pumpage estimates within a continuous range can be developed. The weights used in the development of curves A and B in figure 8 represent two reasonable interpretations of the pumpage data, and other pumpage data were not considered. The problem remains, however, to choose which of these pumpages to use in the calibration of the model. A discussion of this is held until later.

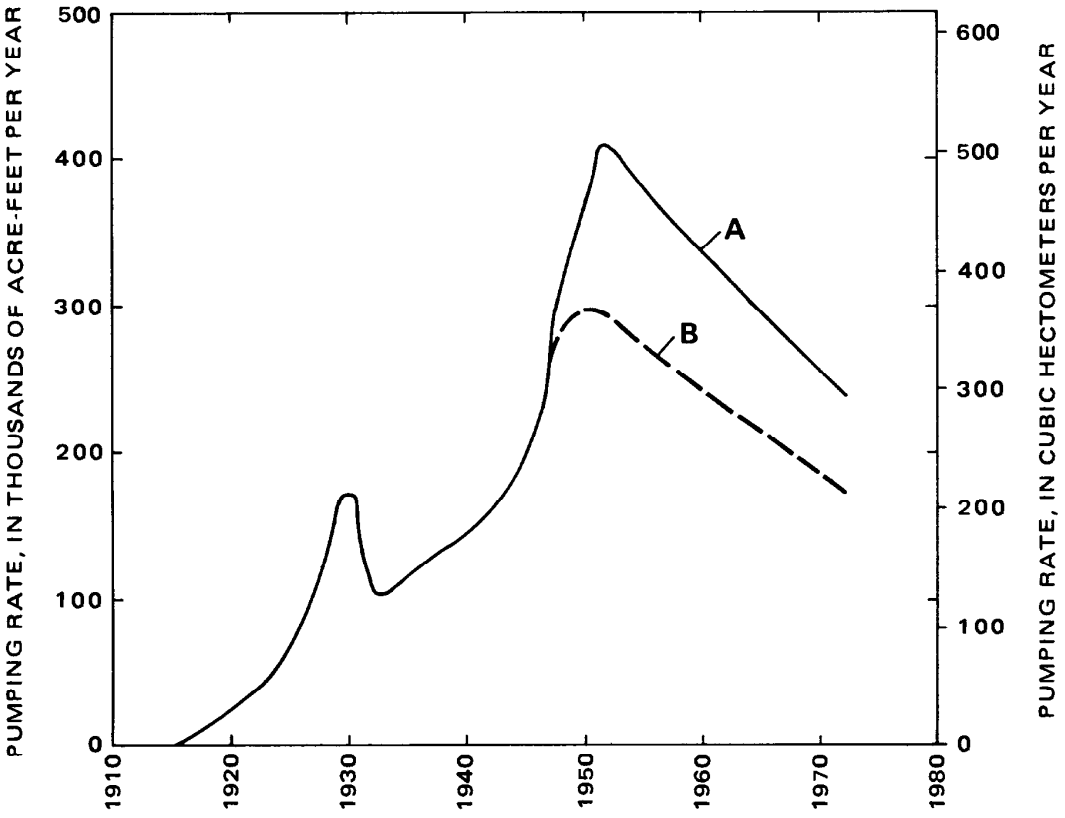

FIGURE 8.—Alternative temporal distributions of pumpage for possible use in the mathematical model. Curve A is the average of all data shown in figure 7. Curve B is the average of curves A, B, and C in figure 7.

IRRIGATION RETURN

When land is being irrigated, water in excess of the moisture requirement of crops is applied to control the salt level in the root zone. The question arises as to the fate of water that gets below the root zone. If part of the applied water percolates downward until it reaches the zone of saturation, it becomes available for reuse.

A necessary input to the model is the quantity of water returned to the zone of saturation. Estimates of irrigation return are necessarily linked with estimates of pumpage, which was discussed in the previous section. Snyder (1955) estimated that in Antelope Valley about 70 percent of the applied water is actually consumed by the crop or otherwise lost and that the mean annual application of water to the irrigated lands is about 6 ft (1.8 m). Correspondingly, the mean annual percolation past the root zone is about 2 ft (0.6 m). This percolate moves generally downward through the unsaturated zone toward the water table. Two separate lines of evidence, however, suggest that by about 1955 most of this water had not reached the water table.

The first line of evidence involves a consideration of the historical trend of the dissolved-solids concentration in water below the water table. If the irrigation-return percolate, which has a dissolved-solids concentration of about 700 mg/l (milligrams per liter) (R. E. Lewis, written commun., 1976), is mixing with water below the water table, which from 1908 through 1955 had a concentration of about 250 mg/l (Johnson, 1911; Koehler, 1966; Moyle, 1965), the concentration below the water table probably should have increased with time. For 1908 through 1955, however, a general increase in dissolved-solids concentration was not observed (fig. 9), which tends to support the assumption that by 1955 the irrigation-return percolate had not reached the water table. During the 1960's the concentration did increase, suggesting that during that period the percolate began to mix with ground water.

The second line of evidence involves the existence of perched ground-water bodies. The presence of perched ground water in Antelope Valley is indicated by falling water in some wells. The development of perched ground-water bodies indicates the presence of subsurface geologic conditions that retard the downward movement of the irrigation-return percolate. Thus, the perched ground-water bodies provide the mechanism for the retention of irrigation-return percolate above the water table.

The evidence supporting the assumption that most of the percolate was retained above the water table during the model calibration period, 1915 through 1961, is not conclusive, and significant uncertainty exists as to the true state of the prototype. The resolution of this uncertainty is discussed in the following section.

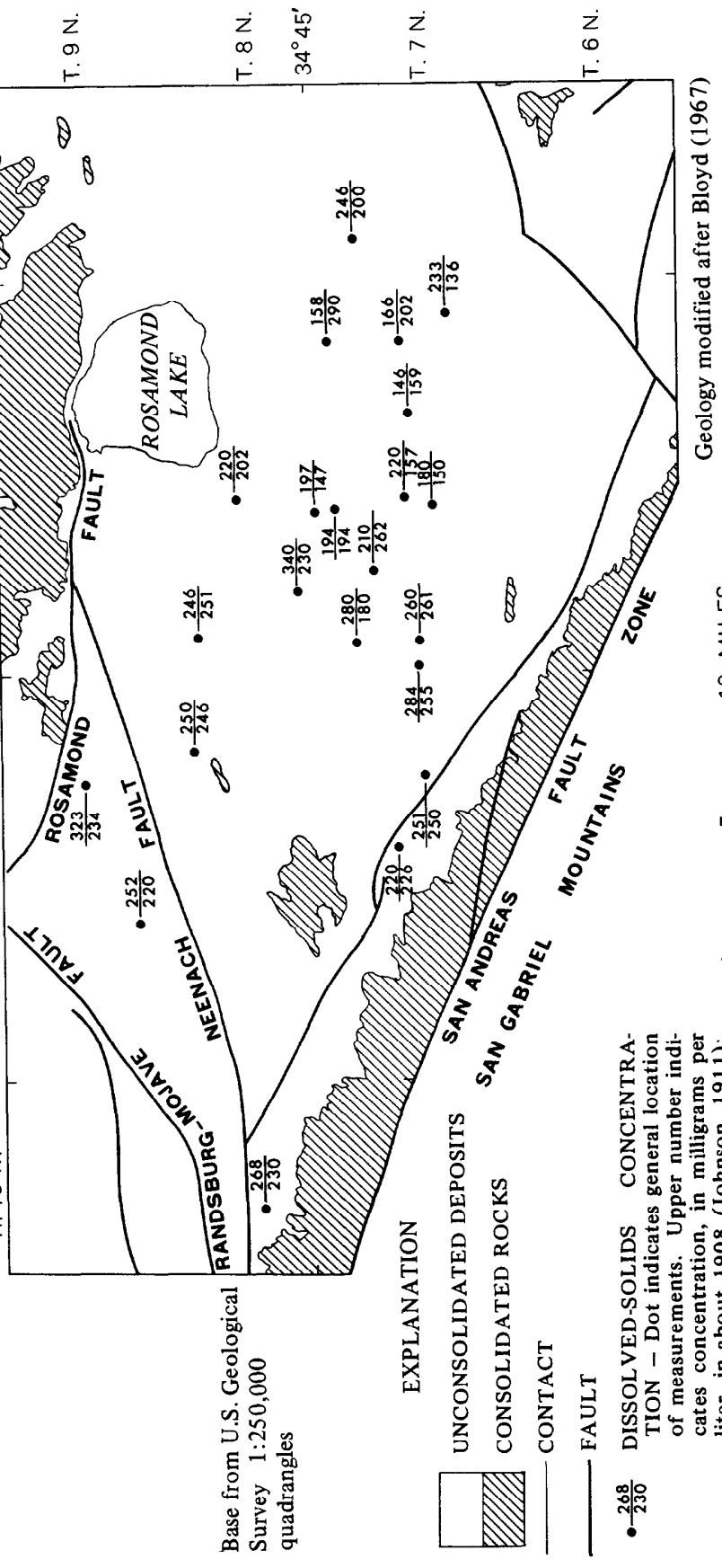

FIGURE 9.—Part of Antelope Valley, Calif., showing comparison of ground-water quality for 1908 and 1955.

SELECTION OF NET PUMPAGE FOR MODEL CALIBRATION

The pumpage that is actually input to the model is the net pumpage, which is the quantity of water extracted from wells minus the quantity of irrigation return that reaches the water table. Significant uncertainty exists regarding both of these quantities, and a possible consequence of using the wrong net pumpage in the model calibration is storage-coefficient values that deviate from the true values. The following section describes the decision process used to select, from a limited number of alternatives, the net pumpage that probabilistically is nearest to the true net pumpage.

If the true state of the prototype were known, the consequence of using a given net pumpage could be determined. Under uncertainty, however, the consequence cannot be determined simply because the state of the prototype is not known for certain, and thus it is necessary to use the concept of expected value. The expected value of the consequences of a decision is the weighted sum of the consequences of the decision for the various states of nature. The weights are the probabilities that a particular state is realized in the prototype. For each net pumpage it is possible to compute the expected consequence, and the best decision is the decision with the smallest expected consequence. An index of the consequence of using a particular net pumpage is the deviation of the pumpage from the true pumpage. The best pumpage to use, then, is the one for which the expected value of the deviation is the least.

The possible pumpages are defined as P_1 and P_2, which symbolically represent pumpage curves A and B in figure 8. The possible irrigation returns are defined as R_1 and R_2, which represent full irrigation return to the water table and no irrigation return. Thus, there are four possible joint states of the ground-water basin; P_1 can occur with either R_1 or R_2, and P_2 also can occur with either R_1 or R_2. For 1950 through 1961 the net pumpages P_1R_1 (where P_1R_1 symbolically represents the joint occurrence of P_1 and R_1) and P_2R_2 are about equivalent because P_1 equals about 1.4 P_2. P_1 and P_2 are assumed to be equally likely true states of the prototype. Similarly, R_1 and R_2 are assumed to be equally likely true states of the prototype. It follows, if the pumpage and irrigation states occur independently, the joint occurrence of any of the possible combinations of pumpage and irrigation return is equal to one-fourth.

A way of presenting decisionmaking problems involves the use of tree diagrams. In figure 10 a tree diagram for the selection of the net pumpage to use in the calibration of the model is presented. The point at the left-hand node of the diagram represents the initial position, and the four branches of the tree emanating from that point represent the four decisions in the problem. Thus, the left-hand fork is called a

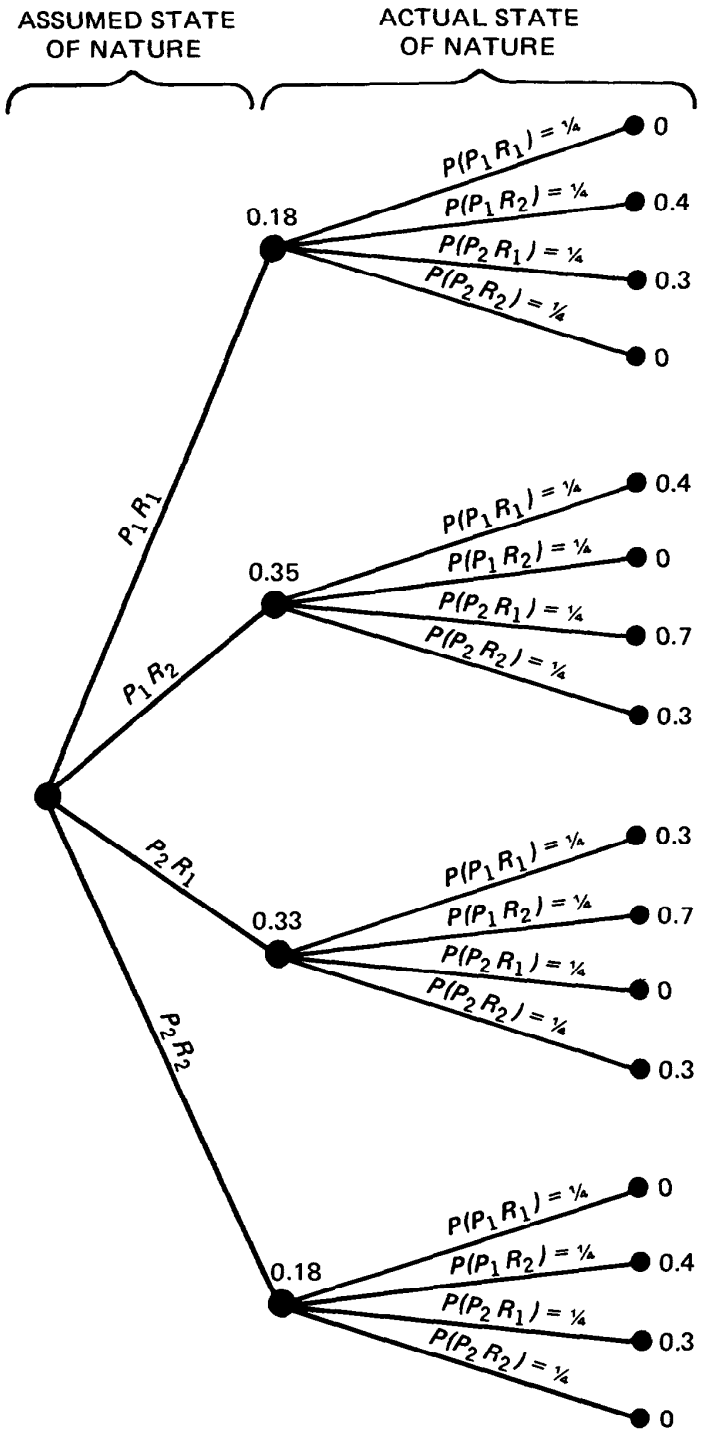

FIGURE 10.—Decision tree showing selection of net pumpage for calibration of transient-state model.

decision fork. At the end of each of the four branches representing the possible decisions, there is another fork with four branches. These four branches represent the possible states of the ground-water basin, and these forks are called state forks.

The numbers on the state branches are the probabilities of the states. The numbers on the right-hand side of the tree diagram are the relative deviations of the assumed net pumpage from the true net pumpage under the realization of a particular state. For example, if the decision is taken to use net pumpage P_1R_1 in the model calibration, but the true state of the prototype is net pumpage P_1R_2, the consequence is the deviation of assumed pumpage from the actual pumpage by the relative amount 0.4. The numbers at the state forks are the expected values of the deviation.

At the decision fork, the net pumpages P_1R_1 and P_2R_2 have the lowest expected deviation. Pumpage P_1R_1 represents pumpage curve A in figure 8 combined with an irrigation return equal to 30 percent of the pumpage. Pumpage P_2R_2 represents pumpage curve B in figure 8 combined with no irrigation return.

The above analysis applies only for 1950 through 1961. The results of a similar analysis for 1915 through 1949 indicate that all the net pumpages have equal expected deviations. If the probability of no irrigation return during 1915 through 1949 is greater than one-half, however, which would be a reasonable assumption given the assumption of equal likelihood for 1950 through 1961, the decision analysis indicates that net pumpages P_1R_2 and P_2R_2 (which are similar net pumpages because curves A and B in figure 8 coincide for much of the period 1915 through 1949) produce the smallest expected deviation of the assumed pumpage from the true pumpage.

The equal likelihood for all possible states was assumed in the analysis. P_2 is probably a more likely state of the prototype than P_1, however. Likewise, R_2 is probably a more likely state than R_1. The revision of the analysis with probabilities reflecting these subjective evaluations clearly indicates the use of net pumpage P_2R_2 in the calibration of the transient-state model. This net pumpage was in fact used.

REDUCTION OF NATURAL DISCHARGE

Natural discharge of ground water by evapotranspiration is greatest if the water table is near the land surface. If the position of the water table moves downward, the rate of natural discharge is suppressed. If the water table moves beyond the reach of roots of plants, natural discharge by evapotranspiration will become insignificant.

Pumping from the Antelope Valley ground-water basin has caused lowering of the water table and, consequently, the suppression of natural discharge. Field data are not available on the effects of water-level declines on the level of natural discharge, but operation of the model indicates that this discharge may have ceased in about 1950 (fig. 11). The mass balance for the Antelope Valley ground-

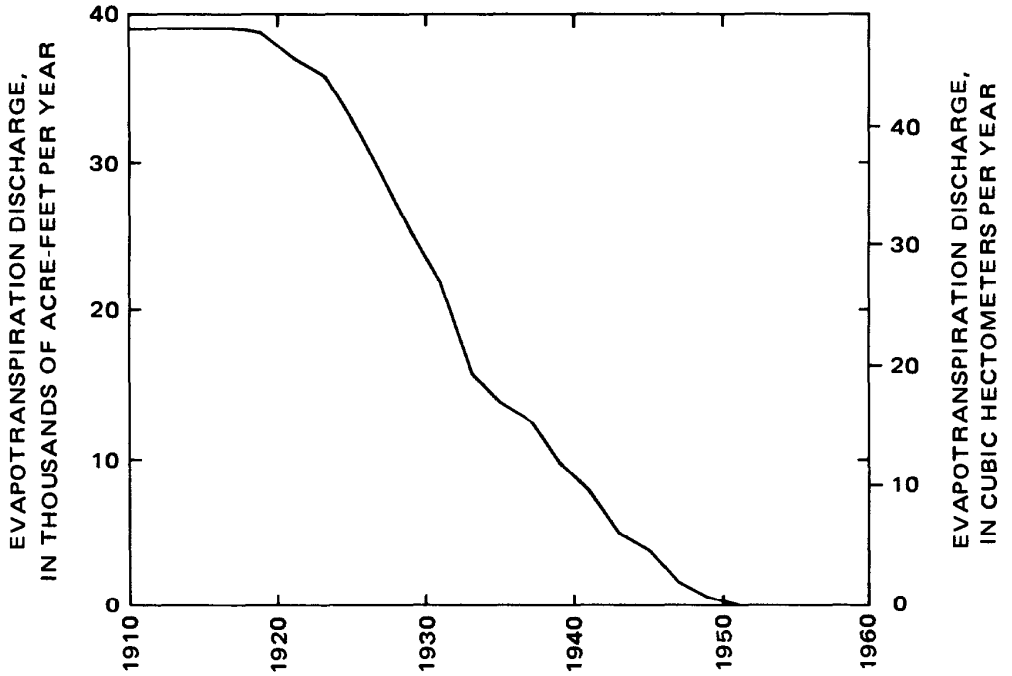

FIGURE 11.—Reduction of evapotranspiration computed by the mathematical model.

water basin indicates that the annual discharge of ground water by evapotranspiration may have been about 39,400 acre-ft (48.5 hm^3) in 1915.

Theoretical research on the discharge of ground water by evapotranspiration has been restricted to determining the annual use of water by different plant species when the depth to the water table does not change greatly with time. Very little is known about the quantitative effects of large temporal changes in the depth to the water table. Prediction of changes in the use of ground water is difficult because roots of established plants may, to a limited extent, keep pace with a declining water table, especially if the depth to the water table increases slowly. This phenomenon has not been quantified by researchers, however. Therefore, its possible occurrence was ignored in the construction of the model. The relation shown in figure 3 was assumed to relate temporal changes in evapotranspiration discharge to temporal changes in the depth to the water table, even though the relation shown in figure 3 actually applies only to the case of a time-invariant depth to the water table.

CALIBRATION OF THE TRANSIENT-STATE MODEL

The transient-state model was calibrated to the prototype water levels for 1961. Hydraulic heads that were computed for 1915 by the mathematical model were used as initial conditions, and the model simulated changes in hydraulic heads for 1915 through 1961. For

operation of the model, this period was divided into 235 time steps, each of 73 days. The pumpage for a given year (fig. 7) was assumed to be distributed uniformly throughout the year.

Even though a large number of water-level observations are available (Dutcher and others, 1962; Moyle, 1965; Koehler, 1966), accurate potentiometric maps of the principal and deep aquifers cannot be constructed from field data. Intraaquifer confining members occur in both the principal and deep aquifers (a condition that was not considered in the conceptual model), and differential pumping from between these members has caused the development of vertical hydraulic-head differentials within the aquifers. Head differentials of as much as 80 ft (24 m) in places occur over a vertical interval as small as 400 ft (120 m). In the principal aquifer, the heads in shallow wells are typically higher than heads in deeper wells; however, in some areas this situation is reversed. Consequently, the indicated head at a point in the potentiometric map (pl. 3) is intended to represent the average head over the saturated thickness of the aquifer at that point.

The calibration procedure was started by making initial estimates of the storage coefficient of the principal and deep aquifers. Using lithologic logs for wells, geologic data, and laboratory tests of similar deposits, Bloyd (1967) estimated the storage coefficient of the principal aquifer and of the deep aquifer for areas where the deep aquifer is unconfined. For the applicable areas these estimates were used as initial estimates of the storage coefficient in the calibration procedure. In the area where the deep aquifer is confined, the storage coefficient of the deep aquifer was estimated by using the rule of thumb that the ratio of the storage coefficient to the aquifer thickness is about 10^{-6} per foot (3×10^{-6} per meter) (Lohman, 1972). The average thickness of the aquifer in the confined area is about 1,000 ft (300 m), and a storage coefficient of 0.001 for this area was used in the model.

The transmissivity of the principal and deep aquifers and the vertical hydraulic conductivity of the lacustrine deposits were obtained from the calibration of the steady-state model and were used in the transient-state model. These parameters were invariant during the calibration of the transient-state model; hence, the objective of this calibration was to fit the transient-state model to the prototype water levels by adjusting the storage coefficient. Only the storage coefficients of the principal aquifer and of the deep aquifer where it is unconfined were adjusted during the calibration.

Plates 11 and 12 show the final storage coefficients for the principal and deep aquifers. The storage coefficients do not deviate significantly from the initial estimates (fig. 4).

Hydrographs of computed hydraulic heads and measured water levels in the principal aquifer are shown in figures 12 and 13. The

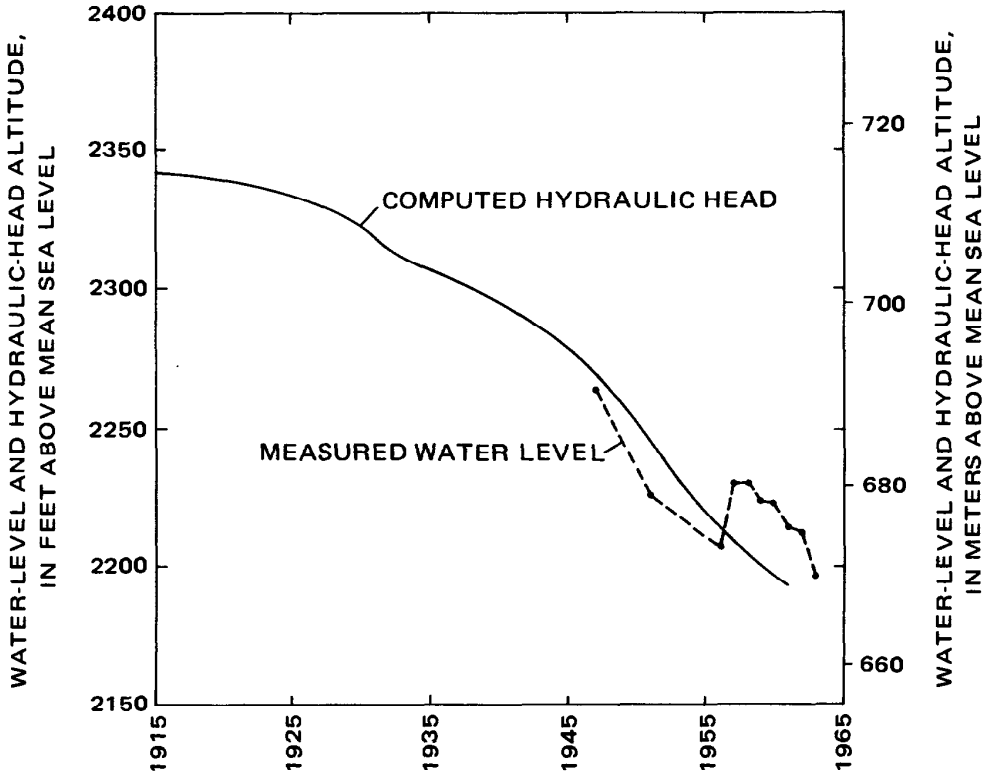

FIGURE 12.—Hydrographs of computed hydraulic heads in the principal aquifer at node 144 and measured water levels in well 8N/13W–11Q1. Water-level measurements are from Moyle (1965).

hydraulic heads were computed by the mathematical model using the storage-coefficient distributions given on plates 11 and 12 and the transmissivity distributions given on plates 7 and 8. Plate 13 shows the geographic variation of hydraulic heads in the principal and deep aquifers that were computed by the mathematical model. The general shape of the computed solution compares well with the potentiometric map of the prototype water levels shown on plate 3; however, the areas of low hydraulic head that are associated with areas of concentrated pumpage are more disperse in the computed solution than those observed in the prototype. Considering all areas of the ground-water basin, the area-weighted median absolute deviation of the computed hydraulic heads from the prototype water levels was 25 ft (7.6 m) (fig. 5).

DESCRIPTION OF MODELING ERRORS

SOURCES OF ERROR

The observed deviation of the computed hydraulic heads from the prototype water levels is the result of errors associated with the conceptual model, the computational scheme, the system parameters, the

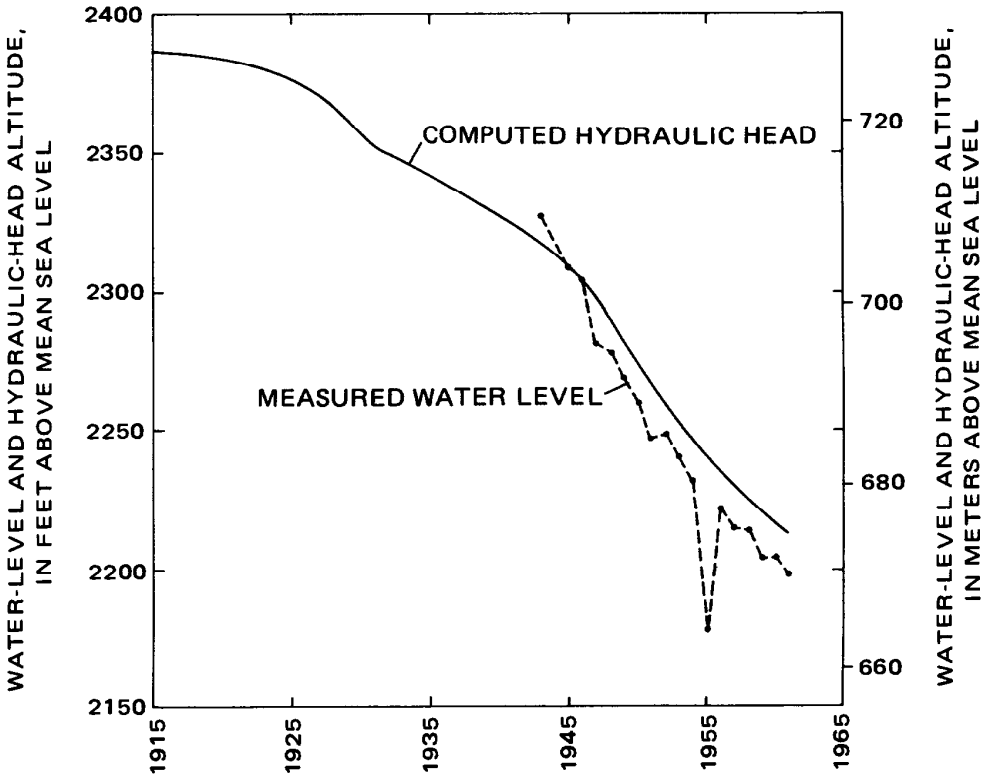

FIGURE 13.—Hydrographs of computed hydraulic heads in the principal aquifer at node 248 and measured water levels in well 7N/11W–28E1. Water-level measurements are from Koehler (1966).

input data, the initial conditions, and the prototype water levels. Table 2 gives a subjective assessment of the relative importance of these sources of error in explaining the observed deviations.

TABLE 2.—*Importance of various possible sources of the deviation of the computed water levels from the prototype water levels*

Source of error	Relative Importance	
	Steady-state model	Transient-state model
Conceptual model	Low	Intermediate
Computational scheme	Low	Low
System parameters	Low	Low
Input data	Intermediate	High
Initial conditions	None	Intermediate
Prototype water levels	High	High

Conceptual model

The errors associated with the conceptual model are errors that result mainly from the simplifying assumptions used in the conceptualization of the prototype. Although errors of conceptualization are probably not large compared to other errors in the model, these errors result mostly from the assumption that intraaquifer ground-water

flow is strictly horizontal and that the transmissivity of the principal aquifer is time invariant.

Computational scheme

Errors associated with the computational scheme are errors resulting from the numerical approximation of the solution to the governing equations. The numerical solution converges to the true solution as the elements are reduced to zero area (Hutton and Anderson, 1971). The use of elements with nonzero area results in the departure of the numerical solution from the true solution, especially where large changes in hydraulic-head gradients are involved. The computation scheme is not a serious source of error in the model, however.

System parameters

The system parameters consist of the transmissivity and storage coefficient of the principal and deep aquifers and the vertical hydraulic conductivity of the lacustrine deposits. Prior estimates of these parameters are refined during the calibration of the model. The objective of the calibration is to identify parameter values that minimize the deviation of the computed hydraulic heads from the measured water levels while keeping the parameter values within physically reasonable limits. It is difficult to recognize when minimum-deviation parameter values have been found, however, and the calibration procedure is usually terminated prematurely. The presumption always remains that, if additional calibration runs had been made, perhaps the fit of the model to the prototype water levels could have been improved.

In using the model to make predictions of the response of the prototype to specified inputs, errors associated with the system parameters result from the deviation of the system parameters from their true values. Relatively small adjustments were made to the system parameters during the calibration of the steady-state and transient-state models. A consistency exists between estimates of the system parameters obtained from field data and estimates obtained from the calibration procedures. Consequently, the probability that the system parameters used in the model are close to the true parameters is greater than if that consistency did not exist.

Nevertheless, uncertainty as to the actual pumpage and irrigation return creates a corresponding uncertainty as to the adequacy of the storage-coefficient values obtained from the calibration of the transient-state model. Although not previously discussed, the actual natural recharge to the ground-water basin is known uncertainly, which creates uncertainty as to the adequacy of the transmissivity values obtained from the calibration of the steady-state model.

If different estimates of the state of the prototype had been used in the calibration, different estimates of the system parameters probably would have been obtained. Figures 14 and 15 show the effects that changes in the system parameters would have on the predictions of hydraulic head that are made with the model. Figure 14 shows the effects on the computed hydraulic heads of relative changes in the storage-coefficient values. The measure of the effect on the computed hydraulic heads is the relative deviation of the computed changes in hydraulic heads at the end of a 20-year simulation period. The maximum and the median deviation are indicated in figure 14. Correspondingly, figure 15 shows the effects on computed hydraulic heads of relative changes in the transmissivity values.

The maximum relative deviation is quite sensitive to changes in the system parameters. The maximum relative deviation, however, is

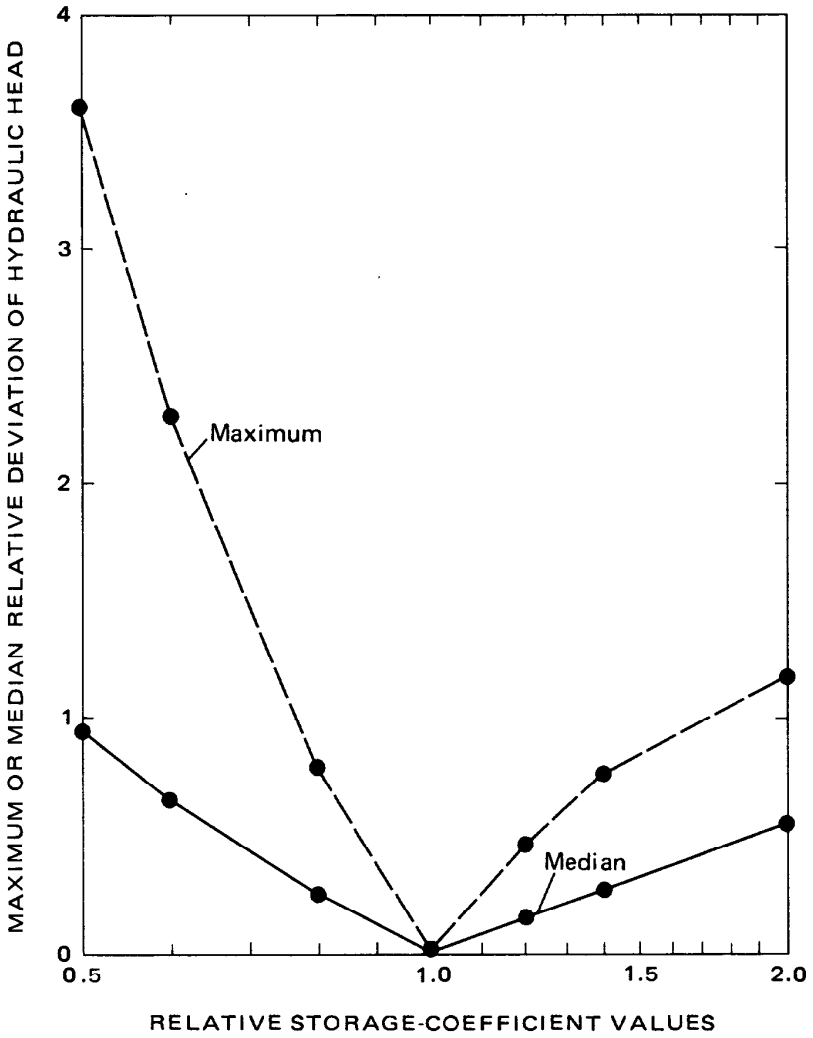

FIGURE 14.—Sensitivity of computed hydraulic heads to changes in the storage-coefficient values used in the model.

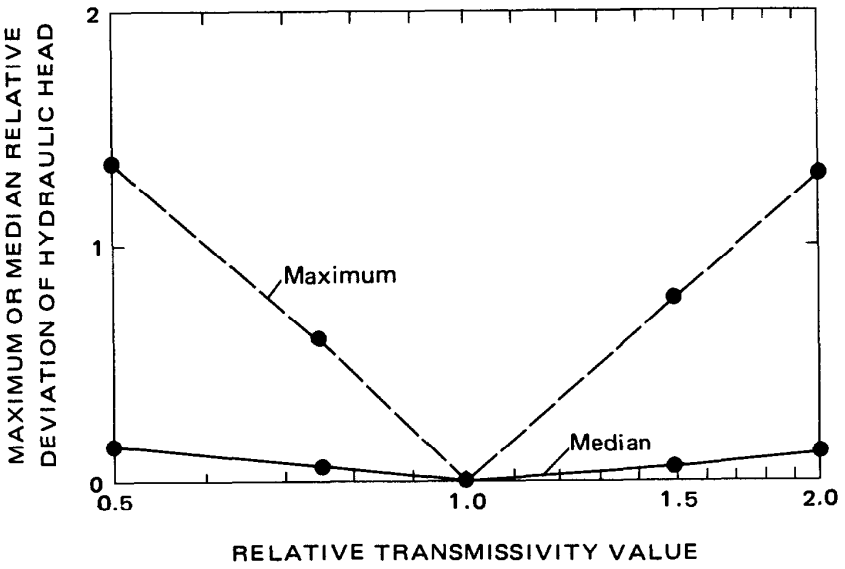

FIGURE 15.—Sensitivity of computed hydraulic heads to changes in the transmissivity values used in the model.

generally associated with areas that have smaller head changes. The median deviation is less sensitive to changes in the system parameters than is the maximum deviation. This is especially true for changes in transmissivity.

Input data

Errors associated with the input data are errors that result from the estimation of natural recharge, natural discharge, pumpage, and irrigation return. Techniques used to obtain these estimates typically bias the estimates, and the bias is for the most part transferred to the system parameters during the calibration process. This may be a relatively important error source.

Initial conditions

Operation of the transient-state model requires specification of initial hydraulic heads. Errors in the initial hydraulic heads produce errors in the computed hydraulic heads. In general, however, these errors become less important as the duration of the period of simulation increases.

Prototype water levels

Errors associated with the prototype water levels are errors of measurement, sampling, and interpretation. The largest errors of measurement probably result from locating wells incorrectly and thereby incorrectly estimating the altitude of the land surface at the well from topographic maps. Some water-level measurements may not be

representative of the aquifer. Measurement of water levels in wells that are being affected by local pumping or in wells tapping perched water bodies, for example, will not be representative of aquifer conditions. These are sampling errors. Interpretation errors arise where field data are contoured or extrapolated to areas without any data. Prototype water levels probably are a serious error source.

ERRORS OF PREDICTION

The predictive accuracy of the model, when measured in terms of the deviation of the computed hydraulic heads from the prototype water levels, is directly proportional to the magnitude and duration of pumping. The greater the pumpage or the longer the duration of pumping, the greater will be the probable errors in computed hydraulic heads. If the future magnitude and duration of pumping are similar to those used in the calibration of the transient-state model, the deviation of the computed hydraulic heads from the prototype water levels that were obtained from the calibration of the transient-state model is probably indicative of the predictive accuracy of the model. It may be possible, however, to improve the predictive accuracy of the model by selective use.

Consider three questions that can be asked about model predictions:

1. What will be the future pumpage and what will be the response of the prototype to that pumpage?
2. What will be the response of the prototype to any specified pumpage?
3. What will be the differential response of the prototype to two specified pumpages that are defined to be mutually exclusive?

The answer to the first question will contain errors that result from errors in the conceptual model, errors in the system parameters, errors in the initial conditions, and errors in the pumpage. The answer to the second question, however, will not contain errors resulting from errors in the pumpage. The third question eliminates initial conditions from consideration, and the answer to this question will not contain errors that result from either pumpage or initial conditions.

The elimination of pumpage errors from the second question will improve the probable accuracy of the answer to this question relative to the accuracy of the answer to the first question. The additional elimination of initial-condition errors from the third question will improve the probable accuracy of the answer to this question relative to the accuracy of the answers to both the first and second questions. Therefore, the best predictions are made with the model for interrogations involving the differential response of the prototype.

NUMERICAL SOLUTION OF THE GROUND-WATER EQUATIONS

THE GALERKIN-FINITE ELEMENT CONCEPT

To solve numerically the governing equations of ground-water flow, the solution is expressed by a finite number of parameters. Secondly, we transform the equations of ground-water flow into expressions

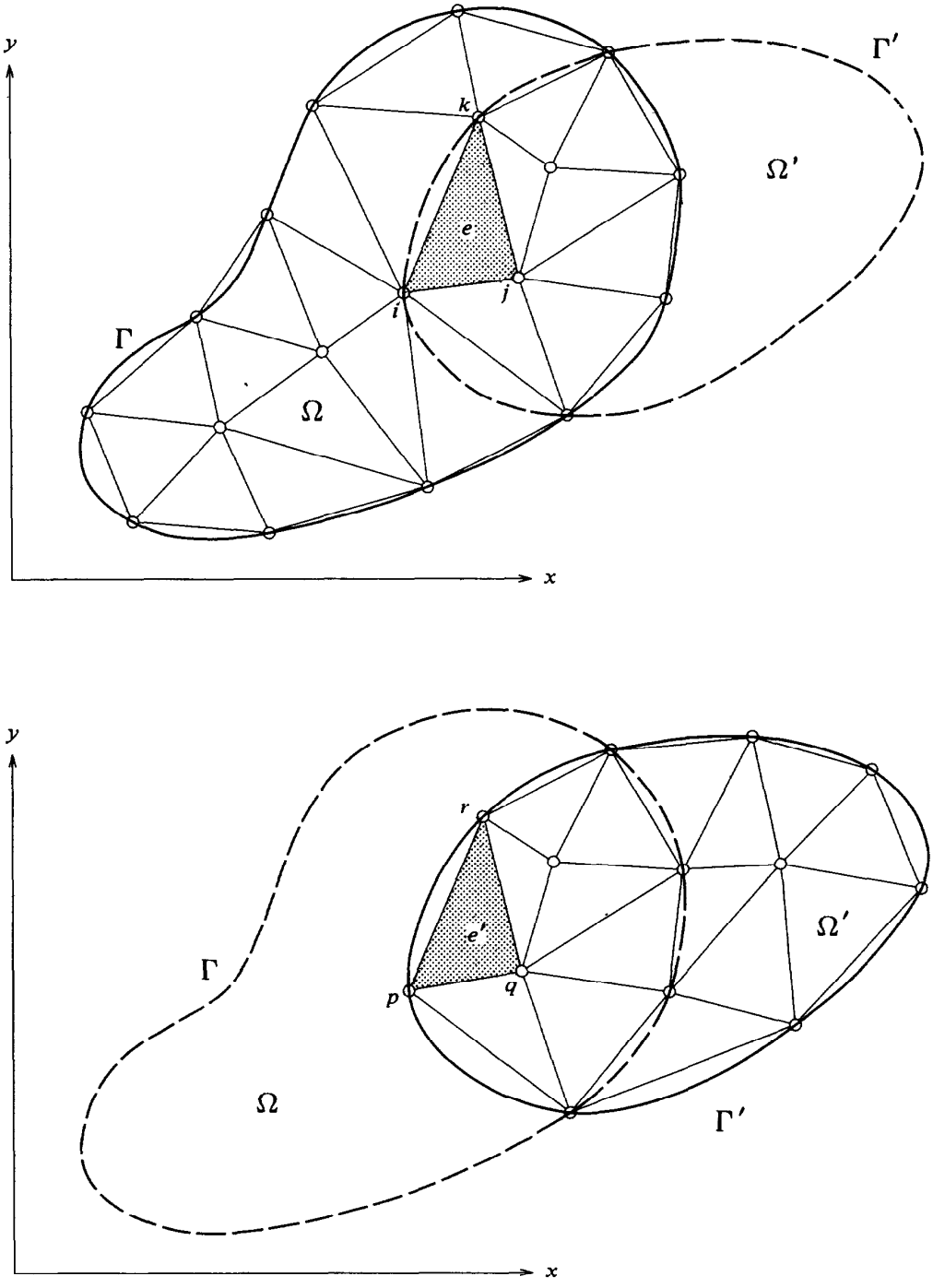

FIGURE 16.—Finite-element discretization scheme used in the mathematical model.

relating these parameters. If the equations are linear, then the relations among the parameters expressing the solution are also linear, that is, we are led to a linear system of algebraic equations. In this process we cannot avoid dealing with a large system of equations. To ameliorate this situation, it is necessary to choose the parameters in such a way that the resulting coefficient matrix is sparse. One method reflecting this feature is the Galerkin-finite element method.

The Galerkin-finite element method was applied to the analysis of single-aquifer ground-water systems by Pinder and Frind (1972). Extension of the Galerkin-finite element method to the analysis of two-aquifer ground-water systems follows. Development of the solution scheme for this system follows the development presented by Pinder and Frind (1972). The difference between their approach and the approach used here results from the selection of a different element shape and the application of the method to a two-aquifer system.

The fundamental idea of the Galerkin-finite element method is to replace a continuous function by values of the function that are specified at a finite number of discrete points called nodes. Function values between these points are calculated using piecewise continuous interpolating functions defined over a finite number of subdomains called elements.

Consider a two-aquifer ground-water system. The first aquifer includes the domain Ω, which is surrounded by the boundary Γ. The second aquifer includes the domain Ω', which is surrounded by the boundary Γ'. The subdivision of this system into triangular elements is shown schematically in figure 16. The domains Ω and Ω' are not everywhere coincident; however, in the areas where these domains are coincident, the elements are also coincident, that is, the nodes i,j, and k respectively have the same locations in the x–y plane as the nodes p, q, and r. The discussion that follows is based in part on the above characteristics of the layout of nodes and elements.

GALERKIN APPROXIMATION

Let us define the linear operators L and L' as

$$L(h) \equiv \frac{\partial}{\partial x}\left(T\frac{\partial h}{\partial x}\right) + \frac{\partial}{\partial y}\left(T\frac{\partial h}{\partial y}\right) - S\frac{\partial h}{\partial t}$$

$$- W - \frac{K}{b}(h - h') = 0 \qquad (5)$$

and

$$L'(h') \equiv \frac{\partial}{\partial x}\left(T'\frac{\partial h'}{\partial x}\right)+\frac{\partial}{\partial y}\left(T'\frac{\partial h'}{\partial y}\right)-S'\frac{\partial h'}{\partial t} - W' - \frac{K}{b}(h'-h) = 0, \quad (6)$$

where x, y are cartesian coordinates,

T is the transmissivity of the first aquifer,
S is the storage coefficient of the first aquifer,
W is the flux of a source or sink in the first aquifer,
h is the head in the first aquifer,
K is the vertical hydraulic conductivity of the confining layer,
b is the thickness of the confining layer,
T' is the transmissivity of the second aquifer,
S' is the storage coefficient of the second aquifer,
W' is the flux of a source or sink in the second aquifer, and
h' is the head in the second aquifer.

Equations 5 and 6 are to be solved in domains Ω and Ω', which are enclosed by the boundaries Γ and Γ'. The boundary conditions are

$$\frac{\partial h}{\partial n} = 0 \text{ on } \Gamma \quad (7)$$

and

$$\frac{\partial h'}{\partial n} = 0 \text{ on } \Gamma', \quad (8)$$

where $\partial/\partial n$ is the outward-pointing normal derivative on Γ and Γ'.

To solve $L(h)=0$ and $L'(h')=0$, we assume trial solutions of the forms

$$h(x,y,t)\simeq\hat{h}(x,y,t)=\sum_{i=1}^{n} C_i(t)\phi_i(x,y) \quad (9)$$

and

$$h'(x,y,t)\simeq\hat{h}'(x,y,t)=\sum_{i=1}^{n'} C'_i(t)\phi'_i(x,y), \quad (10)$$

where $\hat{h}$ and $\hat{h}'$ are series approximations to h and h'; ϕ_i and ϕ'_i are linearly independent trial functions defined over the domains Ω and Ω' and are chosen beforehand. C_i and C'_i are undetermined coefficients, and n and n' are the number of nodal points.

The Galerkin-finite element approximation to equation 5 only will be considered. (It will be shown later how the simultaneous solution to both equations 5 and 6 can be obtained.)

The series approximation to equation 5 will provide an exact representation as n approaches infinity (Forray, 1968, p. 191). For a finite series, the approximation will not exactly satisfy equation 5, and there will be a residual R. The residual is defined by

$$R(x,y,t)=L\left[\sum_{i=1}^{n} C_i(t)\phi_i(x,y)\right]. \tag{11}$$

If the trial solution were the exact solution, the residual would vanish. We attempt to force this residual to zero, in an average sense, through our selection of the undetermined coefficients C_i.

The C_i are calculated by setting the weighted integrals of the residuals to zero. In the Galerkin method (Galerkin, 1915), trial functions are used as weighting functions, that is,

$$\iint_{\Omega} L\left[\sum_{j=1}^{n} C_j(t)\phi_j(x,y)\right]\phi_i(x,y)dxdy = 0. \tag{12}$$

$$i=1, 2,..., n$$

From equation 12 we obtain n linear equations, which can be solved for the n values of C_j.

First, equation 12 can be simplified. By expanding equation 12 we obtain

$$\iint_{\Omega}\left[\frac{\partial}{\partial x}\left(T\frac{\partial}{\partial x}\sum_{j=1}^{n} C_j\phi_j\right)+\frac{\partial}{\partial y}\left(T\frac{\partial}{\partial y}\sum_{j=1}^{n} C_j\phi_j\right)-S\frac{\partial}{\partial t}\sum_{j=1}^{n} C_j\phi_j - W - \frac{K}{b}\left(h'-\sum_{j=1}^{n} C_j\phi_j\right)\right]\phi_i dxdy = 0. \tag{13}$$

$$i = 1, 2,..., n$$

The quantity h′, which occurs in the leakage term of equation 13, can be replaced by the trial solution for h′. By making this substitution into equation 13 we obtain

$$\iint_{\Omega}\left[\frac{\partial}{\partial x}\left(T\frac{\partial}{\partial x}\sum_{j=1}^{n} C_j\phi_j\right)+\frac{\partial}{\partial y}\left(T\frac{\partial}{\partial y}\sum_{j=1}^{n} C_j\phi_j\right)-S\frac{\partial}{\partial t}\sum_{j=1}^{n} C_j\phi_j - W - \frac{K}{b}\left(\sum_{j=1}^{n'} C'_j\phi'_j-\sum_{j=1}^{n} C_j\phi_j\right)\right]\phi_i dxdy = 0. \tag{14}$$

$$i = 1, 2,..., n$$

Equation 14 can be integrated by parts. By assuming transmissivity to be constant over each element and recalling that C_j is a function of time only, we obtain from integration by parts of equation 11 (Pinder and Frind, 1972)

$$\iint_{\Omega}\left[\sum_{j=1}^{n}\left(T\frac{\partial\phi_i}{\partial x}\frac{\partial\phi_j}{\partial x}+T\frac{\partial\phi_i}{\partial y}\frac{\partial\phi_j}{\partial y}+\frac{K}{b}\phi_i\phi_j\right)C_j dxdy+\right.$$

$$\iint_{\Omega}S\phi_i\sum_{j=1}^{n}\phi_j\frac{dC_j}{dt}dxdy+\iint_{\Omega}\phi_i W dxdy-\iint_{\Omega}\phi_i\frac{K}{b}\sum_{j=1}^{n'}C'_j\phi_j dxdy-$$

$$\left.\iint_{\Gamma}\sum_{j=1}^{n}T\frac{\partial\phi}{\partial n}{}_j C_j d\Gamma\right]=0, \qquad (15)$$

$$i=1,2,\ldots,n$$

where $\partial/\partial n$ is the outward-pointing normal derivative on the boundary. Recall that this derivative is everywhere defined to equal zero (eq. 7); therefore, the term containing this derivative vanishes.

The n equations of equation 15 can be written in matrix form as

$$[A]\{C\}+[B]\left\{\frac{dC}{dt}\right\}+[D]\{C'\}+\{F\}=0, \qquad (16)$$

where $[A]$ and $[B]$ are $n\times n$ dimensional matrices; $[D]$ is an $n\times n'$ dimensional matrix; $\{C\}$, $\{dC/dt\}$, and $\{F\}$ are n dimensional vectors; and $\{C'\}$ is an n' dimensional vector. Using terminology from structural engineering, $[A]$ is called the stiffness matrix, $[B]$ is called the dynamic matrix, and $\{F\}$ is called the force vector. The matrix $[D]$ will be called the leakage matrix.

Typical elements of $[A]$, $[B]$, $[D]$, and $\{F\}$ are

$$A_{ij}=\iint_{\Omega}\left(T\frac{\partial\phi_i}{\partial x}\frac{\partial\phi_j}{\partial x}+T\frac{\partial\phi_i}{\partial y}\frac{\partial\phi_j}{\partial y}+\frac{K}{b}\phi_i\phi_j\right)dxdy \qquad (17)$$

$$B_{ij}=\iint_{\Omega}S\phi_i\phi_j dxdy \qquad (18)$$

$$D_{ij}=-\iint_{\Omega}\phi_i\phi_j\frac{K}{b}dxdy \qquad (19)$$

$$F_i=\iint_{\Omega}\phi_i W dxdy. \qquad (20)$$

TRIAL FUNCTIONS

In order to generate the set of algebraic equations represented by equation 16, it is necessary to perform integrations of the trial functions of the form

$$\iint \frac{\partial \phi_i}{\partial x} \frac{\partial \phi_j}{\partial x} dxdy$$

$$\iint \phi_i \phi_j dxdy$$

and

$$\iint \phi_i dxdy.$$

The suitability of the Galerkin approximation for computer application depends on the selection of the trial functions, such that the computational effort for the integrations is minimized.

To facilitate these integrations, the trial functions are defined piecewise in the element sense to obtain global trial functions in the domain Ω. Within an element the approximate solution (equation 9) can be expressed as

$$\hat{h}(x,y) = \sum_{i=1}^{3} C_i(t)\omega_i^e(x,y), \tag{21}$$

where ω_i^e represents local trial functions that are defined only within the element e.

The local trial functions used in this study are linear and are defined on triangular elements. The trial functions are defined such that ω_i^e are nonzero only over element e, equal to unity at the node i, and equal to zero at all other nodes. These functions for the node i (fig. 17) are given by

$$\omega_i^e(x,y) = \frac{1}{2A}\left[(y_j - y_k)x + (x_k - x_j)y + (x_i y_k - x_k y_j)\right]$$

for (x,y) in element e; otherwise,

$$\omega_i^e(x,y) = 0, \tag{22}$$

where A represents the area of the element. Subscripts i, j, k refer to the vertices of the triangular element, and the subscripts progress in counterclockwise order around the element. The area of the element is given by

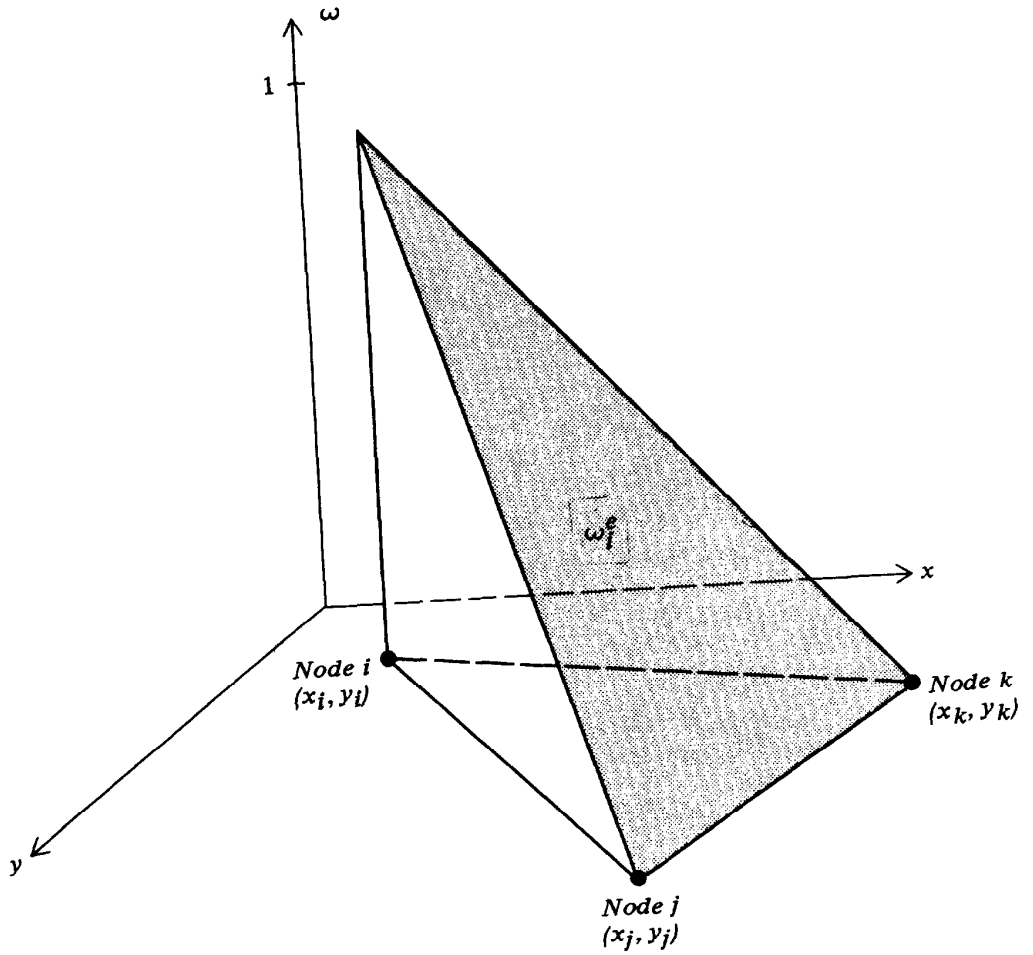

FIGURE 17.—Local trial function used in the mathematical model.

$$A = \frac{1}{2}\begin{vmatrix} x_i & y_i & 1 \\ x_j & y_j & 1 \\ x_k & y_k & 1 \end{vmatrix}. \tag{23}$$

The global trial function ϕ_i is the union of those values of ω_i^e that are found to be nonzero at node i. Thus, the global trial functions are given by

$$\phi_i(x,y) = \omega_i^1 U \omega_i^2 U \ldots U \omega_i^k, \tag{24}$$

where $\{\omega_i^1, \omega_i^2, \ldots, \omega_i^k\}$ is the set of all local trial functions that are nonzero at the node i.

An examination of equation 15 indicates that about $4n^2$ integrations are required. Because the integrals have nonzero values only

where two trial functions share the same element, the number of integrations that actually must be evaluated is much smaller.

INTEGRATION OF THE APPROXIMATING EQUATION

The integrations in equations 17, 18, 19, and 20 are most easily performed on an element basis. Element matrices are generated, and the information is then transferred to the global matrix. Because there are three nodes in an element, each element matrix will be of order three.

Stiffness matrix.

A typical element stiffness matrix [a] will be of the form

$$[a] = T\iint \begin{bmatrix} \frac{\partial\omega_1}{\partial x}\frac{\partial\omega_1}{\partial x} & \frac{\partial\omega_1}{\partial x}\frac{\partial\omega_2}{\partial x} & \frac{\partial\omega_1}{\partial x}\frac{\partial\omega_3}{\partial x} \\ \frac{\partial\omega_2}{\partial x}\frac{\partial\omega_1}{\partial x} & \frac{\partial\omega_2}{\partial x}\frac{\partial\omega_2}{\partial x} & \frac{\partial\omega_2}{\partial x}\frac{\partial\omega_3}{\partial x} \\ \frac{\partial\omega_3}{\partial x}\frac{\partial\omega_1}{\partial x} & \frac{\partial\omega_3}{\partial x}\frac{\partial\omega_2}{\partial x} & \frac{\partial\omega_3}{\partial x}\frac{\partial\omega_3}{\partial x} \end{bmatrix} dxdy$$

$$+ T\iint \begin{bmatrix} \frac{\partial\omega_1}{\partial y}\frac{\partial\omega_1}{\partial y} & \frac{\partial\omega_1}{\partial y}\frac{\partial\omega_2}{\partial y} & \frac{\partial\omega_1}{\partial y}\frac{\partial\omega_3}{\partial y} \\ \frac{\partial\omega_2}{\partial y}\frac{\partial\omega_1}{\partial y} & \frac{\partial\omega_2}{\partial y}\frac{\partial\omega_2}{\partial y} & \frac{\partial\omega_2}{\partial y}\frac{\partial\omega_3}{\partial y} \\ \frac{\partial\omega_3}{\partial y}\frac{\partial\omega_1}{\partial y} & \frac{\partial\omega_3}{\partial y}\frac{\partial\omega_2}{\partial y} & \frac{\partial\omega_3}{\partial y}\frac{\partial\omega_3}{\partial y} \end{bmatrix} dxdy$$

$$+ \frac{K}{b}\iint \begin{bmatrix} \omega_1\omega_1 & \omega_1\omega_2 & \omega_1\omega_3 \\ \omega_2\omega_1 & \omega_2\omega_3 & \omega_2\omega_3 \\ \omega_3\omega_1 & \omega_3\omega_2 & \omega_3\omega_3 \end{bmatrix} dxdy. \qquad (25)$$

Aquifer parameters that appear in the stiffness matrix are assumed to be constant over an element. Because the integration is performed over an element, these parameters are moved from under the integration. The indices used in the element stiffness matrix are local, and they pertain to nodes numbered counterclockwise around the triangle.

The integrations in equation 25 are performed in the global coordinate system. The following integration formulas are used:

$$\iint \frac{\partial\omega_i}{\partial x}\frac{\partial\omega_r}{\partial x}\,dxdy = \frac{1}{4A}(y_{r+1}-y_{r+2})\,(y_j-y_k) \qquad (26)$$

$$r = i,j,k$$

$$\iint \frac{\partial \omega}{\partial y}_i \frac{\partial \omega}{\partial y}_r \, dxdy = \frac{1}{4A}(x_{r+2}-x_{r+1})\,(x_k-x_j) \qquad (27)$$

$$r = i, j, k$$

$$\iint \omega_i \omega_i \, dxdy = \frac{1}{6}A \qquad (28)$$

$$\iint \omega_i \omega_r \, dxdy = \frac{1}{12}A, \qquad (29)$$

$$r = j, k$$

where x_i *and* y_i are the coordinates of the node i.

The global stiffness matrix is obtained by summing, for a given global node, the contribution to that node from each element stiffness matrix. For example, if nodes i and j in the element nodal system correspond to nodes p and q in the global nodal system, the a_{ij} in the element stiffness matrix is added to A_{pq} in the global stiffness matrix. This operational procedure is repeated for each node in an element and for all elements in the domain Ω.

Dynamic matrix.

A typical element dynamic matrix [b] will be of the form

$$[b] = S \iint \begin{bmatrix} \omega_1\omega_1 & \omega_1\omega_2 & \omega_1\omega_3 \\ \omega_2\omega_1 & \omega_2\omega_2 & \omega_2\omega_3 \\ \omega_3\omega_1 & \omega_3\omega_2 & \omega_3\omega_3 \end{bmatrix} dxdy. \qquad (30)$$

The integrals are evaluated using equations 28 and 29, and the global dynamic matrix is assembled according to the operation procedure described previously.

Leakage matrix.

A typical element leakage matrix [d] will be of the form

$$[d] = \frac{K}{b} \iint \begin{bmatrix} \omega_1\omega_1 & \omega_1\omega_2 & \omega_1\omega_3 \\ \omega_2\omega_1 & \omega_2\omega_2 & \omega_2\omega_3 \\ \omega_3\omega_1 & \omega_3\omega_2 & \omega_3\omega_3 \end{bmatrix} dxdy. \qquad (31)$$

As we did for the element dynamic matrix, the integrals in the element leakage matrix are evaluated using equations 28 and 29; however, the assembly of the global leakage matrix is somewhat different. The form of the leakage term arose in part from the introduction of the trial solution for the head in the second aquifer (eq. 10) into equation 13. If nodes i and j in the element nodal system not only

correspond to nodes p and q in the global nodal system for the first aquifer but also correspond to nodes k and m in the global nodal system for the second aquifer, then a_{ij} in the element leakage matrix is added to D_{km} in the global leakage matrix.

Force vector.

The flux term in the force vector arises because of point sources and sinks and because of distributed sinks. Recharge and pumpage are represented mathematically by point sources and sinks. Evapotranspiration discharge is represented mathematically by distributed sinks. Accordingly, the force vector can be expanded to include these flux terms separately. From the expansion, equation 20 is modified to obtain

$$F_i = \iint_{\Omega} \phi_i \sum_{k=1}^{m} Q_k \delta(x - x_k, y - y_k) dxdy + \iint_{\Omega} \phi_i E dxdy, \qquad (32)$$

where

Q_k is the point volumetric recharge to or pumpage from the aquifer,

x_k and y_k are the coordinates of the location of the point source or sink,

δ is the Dirac delta function,

m is the number of point sources and sinks, and

E is the volumetric evapotranspiration discharge per unit area.

Because of the properties of the Dirac delta function (Korn and Korn, 1961, p. 876), the integral

$$\iint_{\Omega} \phi_i \sum_{k=1}^{m} Q_k \delta(x - x_k, y - y_k) dxdy$$

is equal to Q_k, if x_k and y_k are the coordinates of a node. The global force vector is assembled by simply adding Q_k to F_i, where Q_k is located at the node i.

Distributed sinks are handled somewhat differently. The discharge per unit area is given by the relations

$$\begin{aligned} E(x, y) &= E_0 && z < 0 \\ E(x, y) &= E_0 - \frac{E_0 z(x,y)}{z_0} && \text{for } 0 \leq z \leq z_0 \\ E(x, y) &= 0 && \text{for } z > z_0, \end{aligned} \qquad (33)$$

where

E is the volumetric discharge per unit area,
E_0 is the discharge when the water table is at the land surface,
z is the depth below the land surface to the water table, and
z_0 is the depth at which discharge ceases.

The function E can be approximated by using trial functions to interpolate nodal values over an element. The function E is replaced by the series

$$E(x,y) \simeq \sum_{j=1}^{n} E_j \phi_j(x,y),$$

where E_j is the value of E at the node j. The integral

$$\iint_{\Omega} \phi_i E dx dy$$

is then replaced by the integral

$$\iint_{\Omega} \phi_i \sum_{j=1}^{n} E_j \phi_j dx dy.$$

This integral is best evaluated on an element basis. A typical element force vector $\{f\}$ will be of the form

$$\{f\} = \iint \begin{bmatrix} \omega_1\omega_1 & \omega_1\omega_2 & \omega_1\omega_3 \\ \omega_2\omega_1 & \omega_2\omega_2 & \omega_2\omega_3 \\ \omega_3\omega_1 & \omega_3\omega_2 & \omega_3\omega_3 \end{bmatrix} dxdy \begin{Bmatrix} E_1 \\ E_2 \\ E_3 \end{Bmatrix} \tag{34}$$

The integrations in equation 34 are evaluated by using equations 28 and 29. If node i in the element nodal system corresponds to node p in the global nodal system, then the global force vector is assembled by adding f_i in the element force vector to F_p in the global force vector.

FINITE-DIFFERENCE APPROXIMATION OF THE TIME DERIVATIVE

Although the matrices $[A]$, $[B]$, and $[D]$ and the vector $\{F\}$ can now be evaluated, we must still solve the set of ordinary differential equations

$$[A]\{C\} + [B]\left\{\frac{dC}{dt}\right\} + [D]\{C'\} + \{F\} = 0. \tag{16}$$

To do this we approximate the time derivative by using the first-order correct, implicit, finite-difference scheme

$$[A]\{C_{t+\Delta t}\} + \frac{1}{\Delta t}[B]\{C_{t+\Delta t} - C_t\} + [D]\{C'_{t+\Delta t}\} + \{F\} = 0. \quad (35)$$

Equation 35 can be rearranged to obtain

$$\left([A] + \frac{1}{\Delta t}[B]\right)\{C_{t+\Delta t}\} + [D]\{C'_{t+\Delta t}\} = \frac{1}{\Delta t}[B]\{C_t\} - \{F\}. \quad (36)$$

Equation 36 applies to the first aquifer. The parallel expression for the second aquifer is

$$\left([A'] + \frac{1}{\Delta t}[B']\right)\{C'_{t+\Delta t}\} + [D']\{C_{t+\Delta t}\} = \frac{1}{\Delta t}[B']\{C'_t\} - \{F'\}. \quad (37)$$

ASSEMBLY OF THE TWO-AQUIFER SOLUTION

The simultaneous solution of equations 36 and 37 for $\{C_{t+\Delta t}\}$ and $\{C'_{t+\Delta t}\}$ can be obtained by first assembling the matrix equation

$$([\Pi] + \frac{1}{\Delta t}[\Upsilon])\{X_{t+\Delta t}\} = \frac{1}{\Delta t}[\Upsilon]\{X_t\} - \{\Psi\}, \quad (38)$$

where

$$[\Pi] \equiv \begin{bmatrix} [A] & [D] \\ [D'] & [A'] \end{bmatrix}$$

$$[\Upsilon] \equiv \begin{bmatrix} [B] & O \\ O & [B'] \end{bmatrix}$$

$$\{X_t\} \equiv \begin{Bmatrix} \{C_t\} \\ \{C'_t\} \end{Bmatrix}$$

$$\{X_{t+\Delta t}\} \equiv \begin{Bmatrix} \{C_{t+\Delta t}\} \\ \{C'_{t+\Delta t}\} \end{Bmatrix}$$

$$\{\Psi\} \equiv \begin{Bmatrix} \{F\} \\ \{F'\} \end{Bmatrix}$$

Equation 38 can then be solved for $\{X_{t+\Delta t}\}$, which can be easily decomposed into $\{C_{t+\Delta t}\}$ and $\{C'_{t+\Delta t}\}$.

RECURRENCE ALGORITHM

To bring together the concepts outlined up to this point, the solution scheme for obtaining heads in the two-aquifer system at discrete points in space and time will be presented in a stepwise fashion.

Step 1.—Evaluate $[A]$, $[B]$, $[D]$, $[A']$, $[B']$, and $[D']$ and assemble $[\Pi]$ and $[\Upsilon]$.

Step 2.—Assign the initial heads to $\{X_t\}$.

Step 3.—Evaluate

$$[\Pi] + \frac{1}{\Delta t}[\Upsilon].$$

Step 4.—Evaluate $\{F\}$ and $\{F'\}$ and assemble $\{\Psi\}$. The evapotranspiration discharge (eq. 33) depends on the head in the aquifer. Because this discharge is nonlinearly related to the head, equation 38 is also nonlinear. To maintain the linearity of this equation, we can devise a numerical scheme wherein the evapotranspiration discharge is obtained by extrapolating head values from earlier known time levels to the current, unknown, level. An extrapolation based on the latest two calculated heads provides satisfactory results. Notice, however, that we solve this nonlinear system of equations only approximately when using this quasi-linearization procedure.

Step 5.—Evaluate the vector

$$\frac{1}{\Delta t}[\Upsilon]\{X_t\} - \{\Psi\}.$$

Step 6.—Solve equation 38 for $\{X_{t+\Delta t}\}$ by the point iterative successive over-relaxation method (Varga, 1962). $\{X_{t+\Delta t}\}$ then can be easily decomposed into $\{C_{t+\Delta t}\}$ and $\{C'_{t+\Delta t}\}$. Consequently, the previously undetermined coefficients in the trial solutions

$$\hat{h}(x,y,t) = \sum_{i=1}^{n} C_i(t)\phi_i(x,y) \tag{9}$$

and

$$\hat{h}'(x,y,t) = \sum_{i=1}^{n'} C'_i(t)\phi'_i(x,y) \tag{10}$$

are now known, and these solutions can be used to approximate the continuous distribution of heads in the aquifers. Recall that the trial functions were defined such that they are unity at the node for which they are defined and they are zero at every other node. Because of these characteristics of the trial functions, the trial solutions reduce at the nodal locations to

$$\hat{h}(x_k, y_k, t) = C_k(t) \tag{39}$$

and

$$\hat{h}'(x'_k, y'_k, t) = C'_k(t), \tag{40}$$

where x_k and y_k are the coordinates of node k in the first aquifer and x'_k and y'_k are the coordinates of node k in the second aquifer. At the nodal locations, heads in the aquifers are the coefficients C_k and C'_k.

Step 7.—Replace $\{X_t\}$ with $\{X_{t+\Delta t}\}$.

Step 8.—Add Δt to the elapsed time. Then, if Δt has been changed, return to step 3; otherwise return to step 4.

The above cycle is repeated until the desired period of simulation is covered.

SUMMARY

The Antelope Valley ground-water basin, which has a surface area of 900 mi² (2,300 km²) and a thickness of as much as 5,000 ft (1,500 m), consists of two alluvial aquifers separated by fine-grained lacustrine deposits that are as much as 400 ft (120 m) thick. Natural recharge to the ground-water basin occurs mostly by the infiltration of streamflow. The average annual recharge is 40,700 acre-ft (50.2 hm³). Before the extensive use of ground water for agriculture, the ground-water system was in equilibrium, and the recharge equaled the discharge, which occurred mainly by evapotranspiration.

Extensive pumping of ground water has caused the suppression of evapotranspiration of ground water, and pumping is presently the principal means of discharge from the ground-water basin. During the last 50 years, pumping of ground water in excess of natural recharge has resulted in the decline of water levels as much as 200 ft (61 m). Cumulative pumpage for the period before 1973 is about 10 million acre-ft (12,000 hm³).

Part of the applied irrigation water is consumed by the crop, and part percolates below the root zone. A large part of the cumulative percolate may be stored in the unsaturated zone, and the recharge of the zone of saturation by irrigation return may have been small through the end of the calibration period, 1961.

A mathematical model of the ground-water basin was developed on the basis of a simplified conceptualization of the ground-water system. The model was calibrated by comparing the computed hydraulic heads with the corresponding prototype water levels for both steady-state and transient-state conditions. For the steady-state model, the area-weighted median absolute deviation of computed hydraulic heads from the prototype water levels was 12 ft (3.7 m). For the transient-state model, the median deviation was 25 ft (7.6 m).

The data used to calibrate the model contained errors. These errors

in part caused the observed deviation of the computed hydraulic heads from the prototype water levels. The errors contained both systematic and random components. In general, the systematic errors were probably transferred to the parameters during the calibration procedure.

Predictions made with the model will be in error because of the transfer of data errors to the aquifer parameters during the calibration. The predictions will also contain errors that can be related to the initial conditions and assumed future pumpage. If these three types of errors are present, the median error of water-level prediction will probably be about the same as obtained from calibration of the transient-state model, or about 25 ft (7.6m), if a similar magnitude and duration of pumping are considered.

Prediction errors due to initial conditions and the assumed pumpage can be eliminated if the model interrogation is designed to predict the differential response of the prototype to different pumpage characteristics. If the model is interrogated in this manner, the median error of prediction will probably be substantially less than 25 ft (7.6 m).

REFERENCES CITED

Blaney, H. F., Taylor, C. A., and Young, A. A., 1930, Rainfall penetration and consumptive use of water in Santa Ana River valley and coastal plain: California Dept. Public Works, Div. Water Resources Bull. 33, 162 p.

Bloyd, R. M., Jr., 1967, Water resources of the Antelope Valley East-Kern Water Agency area, California: U.S. Geol. Survey open-file report, 73 p.

California Department of Water Resources, 1947, Report to the Assembly of the State Legislature on water supply of Antelope Valley in Los Angeles and Kern Counties pursuant to House Resolution Number 101 of February 16, 1946: 21 p.

———1957, The California water plan: Bull. 3, 246 p.

California State Water Resources Control Board, 1974, Water quality control plan report, South Lahontan basin: 300 p.

Carpenter, E. J., and Cosby, S. W., 1926, Soil survey of the Lancaster area, California: U.S. Dept. Agriculture, 97 p.

Dibblee, T. W., Jr., 1967, Areal geology of the western Mojave Desert, California: U.S. Geol. Survey Prof. Paper 522, 153 p.

Dutcher, L. C., Bader, J. S., Hiltgen, W. J., and others, 1962, Data on wells in the Edwards Air Force Base area, California: California Dept. Water Resources Bull. 91–6, 209 p.

Dutcher, L. C., and Garrett, A. A., 1963, Geologic and hydrologic features of the San Bernardino area, California, with special reference to underflow across the San Jacinto fault: U.S. Geol. Survey Water-Supply Paper 1419, 114 p.

Dutcher, L. C., and Worts, C. F., Jr., 1963, Geology, hydrology, and water supply of Edwards Air Force Base, Kern County, California: U.S. Geol. Survey open-file report, 225 p.

Forray, M. J., 1968, Variational calculus in science and engineering: New York, McGraw-Hill, 193 p.

Galerkin, B. G., 1915, Rods and plates: Vestn. Inzh. Tech. (USSR) rept. 19, p. 897–908. Translation 63–18924, Clearinghouse Federal Sci. Tech. Inf.

Hedman, E. R., 1970, Mean annual runoff as related to channel geometry of selected streams in California: U.S. Geol. Survey Water-Supply Paper 1999–E, 17 p.

Hutton, S. G., and Anderson, D. L., 1971, Finite element method—a Galerkin approach: Am. Soc. Civil Engineers, Mech. Div. Jour., v. 7, no. 5, p. 1503–1520.

Johnson, H. R., 1911, Water resources of Antelope Valley, California: U.S. Geol. Survey Water-Supply Paper 278, 92 p.

Koehler, J. H., 1966, Data in water wells in the eastern part of the Antelope Valley area, Los Angeles County, California: California Dept. Water Resources Bull. 91–12, 17 p., 6 app.

Korn, G. A., and Korn, T. M., 1961, Mathematical Handbook for scientists and engineers: New York, McGraw-Hill, 1130 p.

Lee, C. H., 1912, An intensive study of the water resources of a part of Owens Valley, California: U.S. Geol. Survey Water-Supply Paper 294, 135 p.

Leopold, L. B., and Wolman, M. G., 1957, River channel patterns: braided, meandering, and straight: U.S. Geol. Survey Prof. Paper 282–B, p. 39–85.

Lohman, S. W., 1972, Ground-water hydraulics: U.S. Geol. Survey Prof. Paper 708, 70 p.

Mabey, D. R., 1960, Gravity survey of the western Mojave Desert, California: U.S. Geol. Survey Prof. Paper 316–D, p. 51–73.

Moore, D. O., 1968, Estimating mean runoff in ungaged semiarid areas: Internat. Assoc. Sci. Hydrology Bull. 13, v. 1, p. 29–39.

Moyle, W. R., Jr., 1965, Water wells in the western part of the Antelope Valley area, Los Angeles and Kern Counties, California: California Dept. Water Resources Bull. 91–11, 16 p., 6 app.

Pinder, G. F., and Frind, E. O., 1972, Application of Galerkin's procedure to aquifer analyses: Water Resources Research, v. 8, no. 1, p. 108–120.

Poland, J. F., Piper, A. M., and others, 1956, Ground-water geology of the coastal zone, Long Beach-Santa Ana area, California: U.S. Geol. Survey Water-Supply Paper 1109, 162 p.

Rantz, S. E., 1969, Mean annual precipitation in the California region: U.S. Geol. Survey open-file report, 5 p.

Robinson, T. W., 1958, Phreatophytes: U.S. Geol. Survey Water-Supply Paper 1423, 84 p.

Snyder, J. H., 1955, Ground water in California—The experience of Antelope Valley: Univ. California, Div. Agri. Sci., Giannini Foundation ground-water rept. no. 2, 171 p.

Theis, C. V., 1963, Estimating the transmissibility of a water-table aquifer from the specific capacity of a well, *in* Bentall, Ray, compiler, Methods of determining permeability, transmissibility, and drawdown: U.S. Geol. Survey Water-Supply Paper 1536–I, p. 332–336.

Thompson, D. G., 1929, The Mohave Desert region, California, a geographic, geologic, and hydrologic reconnaissance: U.S. Geol. Survey Water-Supply Paper 578, 759 p.

Varga, R. S., 1962, Matrix iterative analyses: Englewood Cliffs (New Jersey), Prentice Hall, 322 p.

Wright, R. V., 1924, Antelope Valley, California—Report on agricultural, economic, and ground-water situation: Federal Land Bank of Berkeley, 203 p.

Young, A. A., and Blaney, H. F., 1942, Use of water by native vegetation: California Dept. Water Resources Bull. 50, 160 p.